IOP FTC

IOP PUBLISHING JOURNAL OF PHYSICS: CONDENSED MATTER

J. Phys.: Condens. Matter **19** (2007) 412101 (12pp) doi:10.1088/0953-8984/19/41/412101

FAST TRACK COMMUNICATION

Growth–melt asymmetry in ice crystals under the influence of spruce budworm antifreeze protein

Natalya Pertaya[1], Yeliz Celik[1], Carlos L DiPrinzio[1], J S Wettlaufer[2,3], Peter L Davies[4] and Ido Braslavsky[1,5]

[1] Department of Physics and Astronomy, Ohio University, Athens, OH 45701, USA
[2] Department of Geology and Geophysics, Yale University, New Haven, CT 06520-8109, USA
[3] Department of Physics, Yale University, New Haven, CT 06520, USA
[4] Department of Biochemistry, Queen's University, Kingston, ON K7L 3N6, Canada

E-mail: braslavs@ohio.edu

Received 7 August 2007
Published 10 September 2007
Online at stacks.iop.org/JPhysCM/19/412101

Abstract

Here we describe studies of the crystallization behavior of ice in an aqueous solution of spruce budworm antifreeze protein (sbwAFP) at atmospheric pressure. SbwAFP is an ice binding protein with high thermal hysteresis activity, which helps protect *Choristoneura fumiferana* (spruce budworm) larvae from freezing as they overwinter in the spruce and fir forests of the north eastern United States and Canada. Different types of ice binding proteins have been found in many other species. They have a wide range of applications in cryomedicine and cryopreservation, as well as the potential to protect plants and vegetables from frost damage through genetic engineering. However, there is much to learn regarding the mechanism of action of ice binding proteins. In our experiments, a solution containing sbwAFP was rapidly frozen and then melted back, thereby allowing us to produce small single crystals. These maintained their hexagonal shapes during cooling within the thermal hysteresis gap. Melt–growth–melt sequences in low concentrations of sbwAFP reveal the same shape transitions as are found in pure ice crystals at low temperature (−22 °C) and high pressure (2000 bar) (Cahoon *et al* 2006 *Phys. Rev. Lett.* **96** 255502); while both growth and melt shapes display faceted hexagonal morphology, they are rotated 30° relative to one another. Moreover, the initial melt shape and orientation is recovered in the sequence. To visualize the binding of sbwAFP to ice, we labeled the antifreeze protein with enhanced green fluorescent protein (eGFP) and observed the sbwAFP–GFP molecules directly on ice crystals using confocal microscopy. When cooling the ice crystals, facets form on the six primary prism planes (slowest growing planes) that are evenly decorated with sbwAFP–GFP. During melting, apparent facets form on secondary prism planes (fastest melting planes), leaving residual sbwAFP at the six corners of the

[5] Author to whom any correspondence should be addressed.

hexagon. Thus, the same general growth–melt behavior of an apparently rotated crystal that is observed in pure ice under high pressure and low temperature is reproduced in ice under the influence of sbwAFP at ambient pressure and temperatures near 0 °C.

M Supplementary data are available from stacks.iop.org/JPhysCM/19/412101

(Some figures in this article are in colour only in the electronic version)

1. Introduction

Antifreeze proteins protect animals from freezing by binding to extracellular ice and inhibiting its growth [2–5] and by neutralizing ice nucleation agents [6]. They were first observed some 35 years ago in certain fish that can survive in seawater that is colder than the freezing temperature of their blood [7]. Subsequently, AFPs have also been found in arthropods [8–10], plants [11, 12], bacteria [13, 14] and fungi [15]. In addition to the fundamental challenges associated with understanding the mechanisms by which AFPs inhibit ice growth, these proteins represent a promising approach for protecting other fish, crops, and tissues against freezing or freezing damage [16–21]. The generally accepted 'adsorption–inhibition' [2, 22, 23] mechanism for AFP action holds that specific binding of these proteins to an ice surface results in inhibition of ice growth due to the Gibbs–Thomson effect [22]. Specifically, adsorption of AFPs on the ice surface pins the ice crystal surface, forcing the ice to grow between the bound proteins. This constrained growth gives rise to curved microsurfaces [23, 24], thereby lowering the non-equilibrium freezing point of the ice to below the bulk equilibrium melting point. Within the resulting thermal hysteresis gap (TH), ice crystals appear to be kinetically stable, neither growing nor melting [25, 26]. These ice crystals have a characteristic faceted morphology that results from growth inhibition of the planes to which the AFP binds [5]. For example, when the spruce budworm AFP (sbwAFP) is present in a solution, even at micromolar concentrations, ice crystals take a hexagonal shape [27]. This has been interpreted to be the result of AFP affinity for both primary prism and basal planes. However, the crystallographic affinity of most AFPs remains undefined. It has been observed that 'hyperactive' AFPs, including sbwAFP [27], *Tenebrio molitor* AFP (TmAFP) [28], and the hyperactive fish AFP [29, 30], prevent ice crystal growth parallel to the *c*-axis [31]. In contrast, the five 'moderately active' fish AFPs allow growth in the *c*-axis direction. It is possible that all hyperactive AFPs, like sbwAFP, bind to the basal plane [32–34].

The growth–melt asymmetry of ice crystals was first observed for pure ice in a high pressure anvil cell immersed in a temperature controlled bath [1]. Under atmospheric pressure, the ice crystal, when viewed from the same perspective as shown in figure 1, is bounded by a smooth circle and in three dimensions has the form of a disc. As the pressure is increased, the melting temperature decreases, and at the melting temperature of −16 °C, the system passes through a *roughening transition* wherein the circular shape becomes hexagonal due to the formation of facets at the prism orientations [35]. In this region of the phase diagram growth–melt sequences exhibit a rotation or asymmetry [1], namely, while both growth and melt shapes have a hexagonal morphology, the corners appear to be rotated by 30°, as shown in figure 1. The true crystallographic *a*-axes are collinear with the corners on a growth shape that, when melted, appears to rotate. When re-growing the melt shape, the original growth form and hence orientation is recovered. This is understood using the basic kinetics of crystal growth for a crystal near its roughening transition [1].

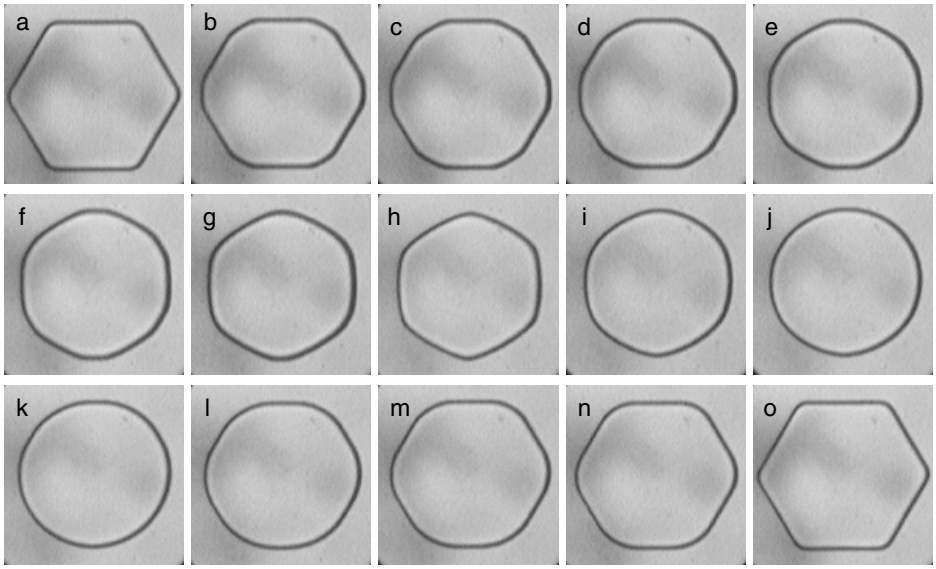

Figure 1. Sequence of melting and growth shapes of an ice crystal in pure water observed in a high pressure anvil cell. The pressure is held at 2000 bar and hence the bulk coexistence temperature is −22 °C. The axis of observation is parallel to the crystallographic *c*-axis, and hence each corner is collinear with one of the *a*-axes and the six prism facets are clearly visible. Starting from the growing shape, which is a hexagonally faceted ice crystal (a), the ice crystal undergoes a series of changes upon slight warming ((b)–(g)) in which it develops a hexagonal shape (g) that is rotated compared to the initial shape (a). On reversing the process by slightly cooling below the melting point, this ice crystal grows again ((i)–(n)) and develops a faceted hexagonal shape (o) that is identical to the starting shape (a) and rotated compare to the melting shape (h). The sequence, which takes 700 s, was taken from [1]. Courtesy of the authors and with permission from APS.

In this communication we examine the growing and melting shapes of ice crystals under the influence of sbwAFP. Additionally, we use a fluorescently tagged sbwAFP to directly visualize sbwAFP in contact with ice. We show that ice crystals in the presence of sbwAFP rotate between growing and melting shapes in a similar manner to the rotation that was found in ice under high pressure. In addition, we show that the proteins accumulate on specific planes and we discuss these findings in the context of our understanding of the basic kinetics of ice-crystal growth.

2. Materials and methods

2.1. Experimental equipment

Two experimental cells were used to contain the control and AFP solutions. In the first cell, a drop of AFP solution was injected in oil that filled a 0.3 mm diameter hole in a temperature controlled metal plate, consistent with the common practice of thermal hysteresis experiments [36]. The second cell, which is similar to the one that was described in [26], is comprised of two coverslips separated by 10 μm and sealed either with parafilm or a silicone elastomer (Sylgard 184, Dow Corning, Midland, MI). The cells were placed in thermal contact with a custom-built temperature controlled stage (figure 2 in [26]). The temperature is monitored with a thermistor and fed back to two thermoelectric cooling elements controlled

by a commercial temperature control device (Newport model 3150 or 3040). We circulate cold water over the warm sides of thermoelectric cooling elements and dry air over the apparatus to keep it free of moisture. This procedure allows the cell temperature to be controlled from room temperature to −40 °C with a precision of ±0.01 °C and a transient response of 0.01 °C in 0.1 s. Samples were imaged using a bright field microscope (Olympus model BH-2), equipped with a 40× LWD objective for video rate imaging, and a Zeiss LSM 510 upright confocal microscope with a long working distance objective (Nikon 50× NA 0.55 ELWD 8.7 mm), and laser illumination lines for fluorescence imaging at 488 and 633 nm. The long working distance air objective allowed simple temperature control of the sample. While allowing for convenient temperature control, this configuration significantly reduced the background compared to wide field fluorescence. The fluorescence signal was detected through a trichroic beam splitter (488/543/633 nm), a secondary dichroic beam splitter (545 nm), and two emission filters: a Cy5 filter (650 nm high pass) and a GFP filter (505–530 nm band pass). There was negligible cross-talk of the Cy5 signal into the GFP filter and vice versa.

2.2. Expression and purification of the GFP-tagged AFPs

The construction and expression of the sbwAFP-GFP, and the isolation and purification of its protein product, are similar to the procedures that are described in [26] for the production of GFP-AFP type III, with a few modifications that are detailed below. The sbwAFP isoform used was 501 [37] because of the ease with which it can be refolded. GFP was linked to the N-terminus of the AFP with a GlyAlaGly linker/spacer between the two fused proteins. Recombinant sbwAFP-GFP expressed in *E. coli* BL21(DE3) was refolded from the insoluble fraction as described for sbwAFP alone [37]. The refolded fusion protein was recovered by ice affinity purification [38] and concentrated by centrifugation in an Amicon ultracentrifugal filter device (Millipore, Billerica, MA).

3. Results

3.1. Growth–melt asymmetry of ice in the presence of sbwAFP: bright field microscopy

Ice crystals are prepared at atmospheric pressure in solutions containing a range of concentrations of sbwAFP, from 0.01 mg ml^{-1} (1.1 μM, TH of 0.02 °C) to 2 mg ml^{-1} (220 μM, TH of 5 °C), in buffer (10 mM tris–HCl, 1 mM EDTA, 5 mM ammonium bicarbonate, pH 8.0). The solutions containing sbwAFP were frozen by rapid quenching to low temperatures (−20 to −40 °C) and then melting back by heating, giving rise to a single individual ice crystal of hexagonal shape. This procedure is the same as the one that has been widely used to measure the activity of AFPs (thermal hysteresis measurements [36]) in which a measurement is made of the difference between the melting temperature and the temperature of explosive crystallization. We made measurements of more than 50 single ice crystals prepared in this manner. For solutions containing high sbwAFP concentrations (>16 μM), and having high thermal hysteresis readings (>0.4 °C), when the non-equilibrium freezing point is reached the explosive phase of crystallization is rapid (>100 μm s^{-1}), taking only a fraction of a second to fill a field of view of 100 μm × 140 μm. In contrast, in solutions containing micromolar concentrations of sbwAFP, and having relatively low thermal hysteresis activity (0.02–0.07 °C), the explosive phase of crystallization is relatively slow, on the order of 3–10 μm s^{-1}. This low thermal hysteresis activity resulted in a more slowly evolving growth–melt process that was observed by simple fine-tuning of the temperature variation. During cooling within the thermal hysteresis gap, the ice crystal maintained its hexagonal

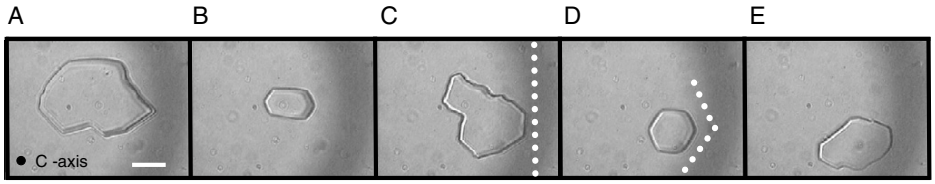

Figure 2. *Growth–melt asymmetry of an ice crystal in a solution containing* 10 μM *spruce budworm ice binding protein: bright field measurements.* (A)–(E) Snapshots from a movie (supplementary materials Movie S1 available at stacks.iop.org/JPhysCM/19/412101) showing the growth and melting of the ice crystal. At the sbwAFP-GFP concentration used (10 μM), the thermal hysteresis is 0.07 °C. The temperature was alternated between 0.02 °C above the melting point of the solution and 0.02 °C below the temperature of rapid crystallization, forcing the ice crystal to melt ((B), (D)) or grow ((C), (E)) in a controlled manner. The images clearly show a 30° shift between the planes of growth and melting of the ice crystal, which causes the ice facets such as the one near the dotted vertical line in (C) to form into corners such as the one near the dotted corner in (D). Scale bar in (A) represents 30 μm.

shape with no observable growth. Cooling to slightly below the non-equilibrium freezing temperature induces growth. The process is discontinuous in character, with periods of rapid growth of several microns interspersed with periods devoid of growth. The growth planes stabilized at an angle of 30° with respect to the initial shape; see Movie 1 in supplementary materials (available at stacks.iop.org/JPhysCM/19/412101). Melting is initiated by raising the temperature approximately 0.01–0.02 °C above the melting temperature. It is then observed that the melt planes stabilized at an angle of 30° relative to the growth planes, causing the crystal to return to the initial hexagonal shape. This growth–melt process of plane rotation was repeated 20–30 times for each single ice crystal studied. Although it was harder to control, growth–melt asymmetry was also observed in solutions with higher sbwAFP concentrations. Snapshots from the movie illustrating the asymmetry of the growth–melt process are shown in figure 2. Behavior similar to that shown in the movie was observed in experiments on more than 50 ice crystals in solutions containing micromolar concentrations of sbwAFP. We emphasize that this ambient pressure behavior under the influence of low AFP concentrations mirrors that of pure ice under high pressure and at low temperature; showing a 30° shift between the growing and melting planes. In control experiments, ice crystals were grown and melted in solutions with no thermal hysteresis activity such as in pure water, 1 M NaCl, 1 mg ml^{-1} GFP and 4 and 20 mg ml^{-1} BSA. In all of these solutions melting shapes were circular. The growth shapes were dependent on the degree of supercooling. For low supercooling, under 0.1 °C, the shapes were circular, but at higher supercooling, such as 0.2 °C, they became hexagonal.

3.2. Visualization of ice growth in a sbwAFP-GFP solution: confocal microscopy

To visualize sbwAFP adsorption onto ice we have produced a recombinant fusion protein consisting of enhanced green fluorescent protein (eGFP) linked to sbwAFP (figure 3(A)). The resulting fluorescent fusion protein, sbwAFP-GFP, shows antifreeze activity similar to that of sbwAFP, and hence can be used to make direct observations of an AFP bound to ice.

In the sbwAFP-GFP visualization experiments using fluorescence microscopy, a thin layer of sbwAFP-GFP solution was rapidly cooled, and the resulting frozen solution was then melted back slowly to the point where it consisted of separate, single-crystal grains with diameters of approximately 10–20 μm. While melting, these crystals take on a hexagonal shape which is maintained during cooling within the thermal hysteresis gap; hence ice crystal growth stops

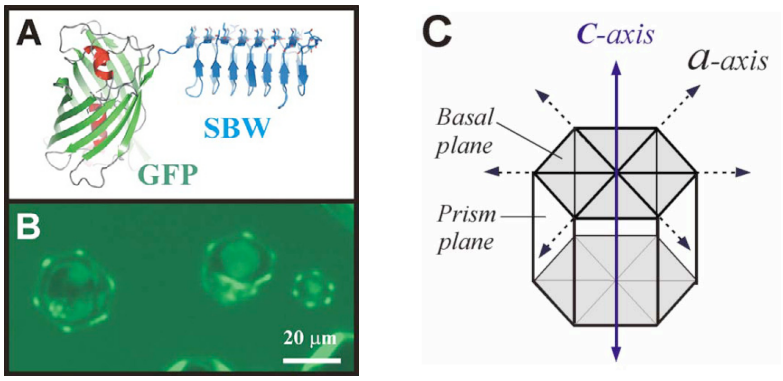

Figure 3. *sbwAFP linked to GFP: fluorescence microscopy.* (A) Ribbon diagram of the spruce budworm ice binding protein (sbwAFP) linked through its N-terminus to the C-terminus of the green fluorescent protein (GFP). (B) Ice crystals decorated with sbwAFP-GFP. The image was taken through a confocal microscope equipped with a GFP fluorescence filter. (C) Diagram of the basal and prism planes of an ice crystal.

until the 'freezing point' is reached. The fluorescence intensity clearly reveals the location of the sbwAFP-GFP on the hexagonal ice crystals (figure 3(B)).

In the system used to examine the binding of sbwAFP-GFP to ice surfaces, the fluorescent protein molecules are present both in solution and on the ice surface. To separate the fluorescence contributions of free molecules in solution from those of ice-bound molecules, we used a procedure previously described in detail [26]. Briefly, the ice crystals are grown in a solution containing sbwAFP-GFP as well as a second dye that is not conjugated to sbwAFP (Cyanine 5-dUTP, Cy-5). Two images are taken of the solution, an image of the non-conjugated dye captured through the Cy-5 filter (figure 4(B)) and an image of the sbwAFP-GFP captured through the GFP filter (figure 4(A)). Then, to reduce the background of the sbwAFP-GFP image, the Cy-5 image is subtracted from the sbwAFP-GFP image (figure 4(C)). This approach relies on the non-conjugated dye neither adhering to the surface of ice, nor being incorporated into the bulk ice. In the images of this particular crystal, no fluorescence was observed on the basal plane, likely due to steric interaction with the glass cover slip of the experimental chamber.

The results of our observations on many crystals reveal that the sbwAFP-GFP molecules adhered to the prism and basal planes. The protein accumulation is maximal at the corners of the melt shapes, which correspond to the centers of the crystallographic primary prism planes that are clearly manifested on the growth shapes. Below we show that this can be understood in terms of the asymmetry of the melting and growth shapes of ice crystals in a sbwAFP solution. The significance of the binding of the proteins to the basal planes of the ice crystals will be discussed elsewhere [32].

3.3. Growth–melt asymmetry in ice crystals under the influence of sbwAFP-GFP

When ice crystals were forced to grow in the presence of sbwAFP-GFP, the growing surfaces were stabilized at close to a 30° angle with respect to the initial (or melting) surfaces, similar to the behavior discussed above for sbwAFP solutions (i.e. without the GFP tag). Every sbwAFP-GFP/ice crystal exhibits this behavior when forced to grow and melt. Following melting, sbwAFP-GFP accumulates at the corners of the hexagonal ice crystal (see figure 5(A)).

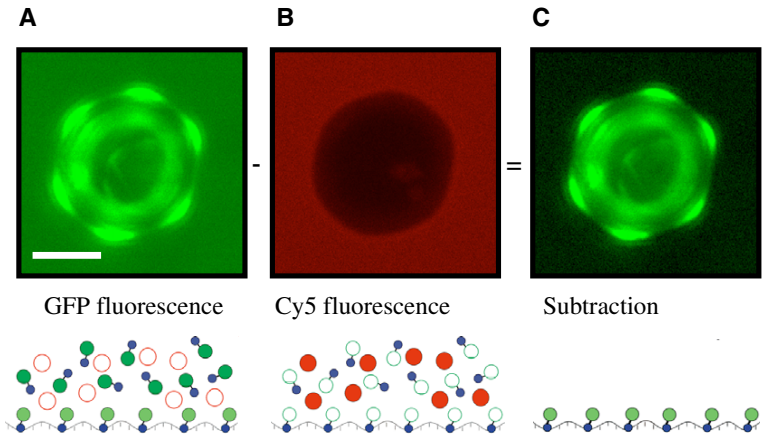

Figure 4. *Image analysis for selective detection of ice-bound sbwAFP-GFP.* Ice crystals were produced in a solution containing sbwAFP-GFP and a free dye (Cyanine 5-dUTP or Cy5) and imaged with 488 and 633 nm illumination lines through two separate fluorescence filters: a Cy5 filter, and a GFP filter. (A) GFP fluorescence alone. White scale bar represents 7 μm. (B) Cy5 fluorescence alone. (C) Subtraction of the Cy5 image from the GFP image. The lower parts of panels (A)–(C) illustrate the molecules present: GFP, large (green) circles in the dumbbells; Cyanine 5, stand alone (red) circles. Filled circles represent molecules detected by fluorescence with a particular optical filter and empty circles denote molecules that are not detected; sbwAFP domains are the small (blue) circles in the dumbbells. The lower parts of the panels were adapted from figure 3(D) in [26] with permission from Biophysical Journal.

During subsequent growth the existing sbwAFP-GFP is overgrown by the ice, and additional AFP molecules from solution attach uniformly to the prism facets that emerge from the melt shape rotated 30° from the planes of the latter (figure 5(B)). In the movie that records melting and growth of ice under the confocal microscope (supplement Movie 2 available at stacks.iop.org/JPhysCM/19/412101), one can see that melting starts at the corners of what was the growth shape and continues until the last region to melt is the center of the facet. This behavior suggests that the bound AFP helps to resist melting of the prism planes relative to the unprotected surfaces (vicinal to the prism planes including the secondary prism planes). If the hexagonal crystal is further melted back, the points of fluorescence disappear completely. But the antifreeze proteins accumulate at the same corners again once the melting process stops, thereby demonstrating again that the six planes of the melt shape are not primary prism planes and that the corners are the prismatic orientation. This is due to the fact that the crystallographic orientation of sbwAFP accumulation is the same during both melting and growth. However, because the corner region of the melt shape encompasses a range of vicinal orientations, the surface concentration falls off with distance whereas the facets on the growth shape represent a single crystallographic orientation and hence have uniform sbwAFP concentration. Therefore we conclude that the sbwAFP adheres to the primary prism planes.

4. Discussion

We observe that ice growth at ambient pressure in the presence of sbwAFP displays the growth–melt asymmetry or apparent rotation of pure ice growing from water at −22 °C and at 2000 bar [1]. Namely, ice crystals have an apparent faceted hexagonal shape both during melting and

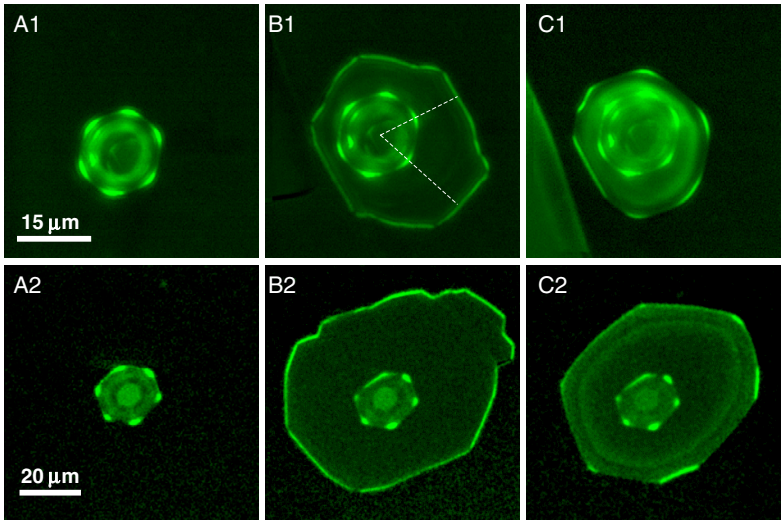

Figure 5. *Growth–melt asymmetry in ice crystals in sbwAFP-GFP solution.* Series 1 and 2, represent the location of the sbwAFP-GFPs on the ice crystals in an sbwAFP-GFP solution. The images are subtraction images as explained in figure 4. (A) Initial melting shapes. (B) Growing shapes. During subsequent growth the sbwAFP-GFPs are overgrown by the ice, and additional sbwAFP molecules from solution attach to the prism facets that emerge from the corners of the melt shape 30° from the planes therein. (C) Partial melting. The crystal appears to have rotated again, with facets becoming corners, and the sbwAFP-GFPs are attached to the same directions as on the original melt shape, accumulating on the centers of the shrinking facets of a hexagonal ice crystal at locations that eventually become corners. A movie of experiment 2 in figure 5 (supplementary materials Movie S2 available at stacks.iop.org/JPhysCM/19/412101) shows the process of growth and melt.

growth but with the planes defining the faces rotated by 30°. In addition, using fluorescently tagged proteins, we found that the AFPs adhere to the corners of the melting crystallites, but adhere to the facets of the growing crystallites. Thus the affinity of the AFP is specific to one direction; the prism direction.

Our description of the process emerges from our understanding of the basic kinetics of the growth/melt process in pure ice near a roughening transition. The apparent rotation of crystals under the shift from growth to melting at high pressures and low temperatures was analyzed quantitatively in terms of the following kinetic processes [1]. The transition from the growth of a hexagonal shape bounded by prism facets to melting begins at the corners, where the molecules are weakly bound and thereby respond immediately by departing the solid (figure 1). Thus, the corners begin to roughen and their rate of recession is substantially larger than that of the facets; the former move approximately 15% of the characteristic crystal size while the latter do not move a discernible distance. The melting of a *finite* facet is not an activated process; molecules detach from the terrace edges and the facet recedes towards its center, uncovering the layer below to repeat the process. Hence, the monolayers bounding the prism facets recede from the corners. Once a corner molecule departs, it exposes a new corner, thereby repeating the process. Therefore, the ratio of the rate of corner formation to the rate of recession of the monolayer across the facet determines the slope of the surface. Clearly visible in figure 1 is an apparently faceted six-sided state in which each 'facet' appears perpendicular to an *a*-axis; a corner on the equilibrium and/or weakly driven growth shape. Therefore, it *appears* as if

the crystal has rotated by 30° but that is illusory as is shown when growth is initiated. Indeed, the 'facets' on the melt shape are dynamically determined as described above, and are in fact molecularly rough, for during growth they move rapidly to reverse the process and restore the faceted equilibrium crystal to its original state.

It is important to note that the asymmetry between the growth and melt shapes is not a peculiarity of ice. For example, it is observed in studies of the crystallization of ^{4}He atoms in the presence of ^{3}He impurities [39]. During growth, the usual faceted hexagonal shapes characteristic of ^{4}He crystals were observed. When the pressure was reduced, however, the melting process occurred from the inside out, leaving the so-called '3D skeleton' of the crystal. During crystal growth, the ^{3}He was incorporated into the solid with a concentration much higher than the equilibrium value either in the bulk liquid or solid. Although the melting pressure of the solid decreases with increasing concentration of ^{3}He, the last parts of the crystal to melt were the ^{3}He corners of the crystal. Detailed descriptions of the roughening transitions [40] and crystallization waves below 0.5 K of ^{4}He crystals are provided in a recent review by Balibar *et al* [41]. They also describe the general observation found in all materials, including ice growing from water [42], that facets grow and melt more slowly than the rough corners, and hence the facets occupy a much greater surface area on growing crystals than on melting crystals.

Evidently, here the AFPs act to shift the step free energy to an equilibrium value at ambient pressure and much higher temperature so as to stabilize the prism plane against roughening. We see a uniformity of AFP coverage on the prism planes of the growth shape, but that the coverage increases on the corners of the melt shapes that were the centers of the facets on the growth shape. We can understand these observations by appeal to the same kinetic processes as described above. The melting of a uniformly AFP covered hexagonal growth shape will begin at the corners, and establish the slope of the surface by the ratio of the rate of new corner formation to the rate of recession of the monolayer across the facet. Hence, the concentration of the AFPs on the corners of the melt shapes is driven by the loss of favorable surface orientations, namely, the prism facets that are eroded from the corners leaving six small favorable regions (and the vicinal orientations flanking them) on the melt shape. Growing back the rough orientations reestablishes the AFP coverage uniformity on the growth shape that is bounded solely by prism planes.

A 30° difference between corner directions in ice growth under the influence of AFPs was noted previously in experiments on antifreeze glycoproteins [43]. In that study, the crystals developed pits on the basal planes that had a hexagonal shape that was rotated 30° relative to the outside hexagonal shape of the crystals. The origin of this rotation was unknown, and it was not evident that it resulted from a melting process. For non-hyperactive AFPs, such as AFP type III, the reported bipyramidal ice crystal shape is a growth shape that emerged from a spherical melted shape [26] and anneals within the thermal hysteresis gap to take on the final form. However, the growth–melt asymmetry might explain some peculiarities in the shapes found in ice crystals grown in the presence of different AFPs, such as the lemon shape of ice crystals grown in solutions containing the TmAFP [44]. In the literature, the crystal shapes observed in experiments using AFPs have been assumed to be the growing shapes [45, 46], and the process by which a crystal was obtained (i.e., melting a large crystal to a typical size of a few tens of microns) was not taken into consideration.

5. Summary

We have shown that when ice crystals are grown or melted in an aqueous sbwAFP solution under ambient pressure, an asymmetry between the growth and melt shapes is observed that

is akin to that seen in pure ice grown from water at low temperature and high pressure. This asymmetry has a fundamental origin in the kinetics of molecular attachment and detachment of water to the ice surface. While the two-dimensional steady melt shapes of ice are bounded by six planes, the planes themselves are not proper facets but rather are rotated 30° with respect to the prism planes of ice. In addition, using fluorescently tagged sbwAFPs, we imaged the proteins bound to the ice crystal surfaces, and showed that the proteins bind to the corners of hexagonal melt shapes whereas during growth the proteins accumulate uniformly on the prism planes that bound the shape.

By comparing the growth–melt asymmetry of high pressure ice formed from pure water with the growth–melt asymmetry of ambient pressure ice formed from a sbwAFP solution, we conclude that the sbwAFPs stabilize the prism direction and that the rotation of the crystal upon melting is a dynamic process that does not require the stabilization of the secondary prism direction. We understand the accumulation of sbwAFP at the corners of the melt shapes to be a dynamical consequence of the kinetics of melting and the uniformity of coverage on the prism orientations of the growth shapes to be a demonstration of the affinity of sbwAFP for that orientation. Furthermore, based on this asymmetry, we suggest that other AFPs might stabilize the melting shape but not the growing shape. Future work will address this hypothesis.

Supplementary materials

Movie S1 Bright field microscopy movie of the growth and melt of an ice crystal in sbwAFP solution, within a solution droplet suspended in oil in the nanoliter-osmometer apparatus. It shows the 30° rotation of the growing shapes compared to the melting shapes.

Movie S2 Fluorescence microscopy movie of growth and melt of an ice crystal in sbwAFP-GFP solution, within a two coverslip thin cell. It shows where the antifreeze proteins accumulate during ice growth and melting.

Acknowledgments

We would like to thank Michael Elbaum and Mike Kuiper for comments on the manuscript and Sherry Gauthier for preparing the sbwAFP-GFP. This work was supported by the Canadian Institutes for Health Research to PLD who holds a Canada Research Chair in protein Engineering, the Bosack and Kruger Foundation and the National Science Foundation (OPP0440841) to JSW, the Condensed Matter and Surface Science program at Ohio University (CMSS) and the Biomimetic Nanoscience and Nanoscale Technology initiative (BNNT) at Ohio University to IB.

Appendix

A.1. Ice structure

Ice Ih is an open structure of water molecules that are connected tetrahedrally by hydrogen bonds. The open structure gives ice unusual characteristics such as the density anomaly, whereby the density of ice is lower than that of water. Ice Ih has a wurtzite structure, wherein three of the four hydrogen bonds participate in a hexagonal arrangement in the basal plane, while the fourth is perpendicular to that plane [31] (see figure 3). A hexagonal prism includes two hexagonal basal planes and six rectangular prism planes each of which are perpendicular to the basal planes. The *a*-axes define the corners between each prism plane and hence are orientated 30 degrees from the normal to each prism plane. When pure liquid water at atmospheric pressure is cooled to slightly below the melting temperature, the crystals formed

are faceted (molecularly smooth) in the '*c*' direction (or on the basal plane) and rough in the '*a* direction, giving a disc shape. At higher supercoolings, dendritic growth occurs along the '*a*' directions. Crystal growth at other planes does not usually occur in pure water solution. The presence of AFP molecules in the solution dramatically affects the growth habits of ice.

References

[1] Cahoon A, Maruyama M and Wettlaufer J S 2006 Growth–melt asymmetry in crystals and twelve-sided snowflakes *Phys. Rev. Lett.* **96** 255502
[2] Davies P L, Baardsnes J, Kuiper M J and Walker V K 2002 Structure and function of antifreeze proteins *Phil. Trans. R. Soc.* B **357** 927–35
[3] Yeh Y and Feeney R E 1996 Antifreeze proteins: structures and mechanisms of function *Chem. Rev.* **96** 601–18
[4] Ewart K V, Lin Q and Hew C L 1999 Structure, function and evolution of antifreeze proteins *Cell Mol. Life Sci.* **55** 271–83
[5] Knight C A and Wierzbicki A 2001 Adsorption of biomolecules to ice and their effects upon ice growth. 2. A discussion of the basic mechanism of 'antifreeze' phenomena *Cryst. Growth Design* **1** 439–46
[6] Du N, Liu X Y and Hew C L 2003 Ice nucleation inhibition—mechanism of antifreeze by antifreeze protein *J. Biol. Chem.* **278** 36000–4
[7] DeVries A L 1971 Glycoproteins as biological antifreeze agents in antarctic fishes *Science* **172** 1152–5
[8] Tomchaney A P, Morris J P, Kang S H and Duman J G 1982 Purification, composition, and physical properties of a thermal hysteresis 'antifreeze' protein from larvae of the beetle, Tenebrio molitor *Biochemistry* **21** 716–21
[9] Graham L A and Davies P L 2005 Glycine-rich antifreeze proteins from snow fleas *Science* **310** 461
[10] Tyshenko M G, Doucet D, Davies P L and Walker V K 1997 The antifreeze potential of the spruce budworm thermal hysteresis protein *Nat. Biotechnol.* **15** 887–90
[11] Urrutia M E, Duman J G and Knight C A 1992 Plant thermal hysteresis proteins *Biochim. Biophys. Acta* **1121** 199–206
[12] Worrall D, Elias L, Ashford D, Smallwood M, Sidebottom C, Lillford P, Telford J, Holt C and Bowles D 1998 A carrot leucine-rich-repeat protein that inhibits ice recrystallization *Science* **282** 115–7
[13] Gilbert J A, Hill P J, Dodd C E and Laybourn-Parry J 2004 Demonstration of antifreeze protein activity in Antarctic lake bacteria *Microbiology* **150** 171–80
[14] Muryoi N, Sato M, Kaneko S, Kawahara H, Obata H, Yaish M W F, Griffith M and Glick B R 2004 Cloning and expression of afpA, a gene encoding an antifreeze protein from the Arctic plant growth-promoting rhizobacterium Pseudomonas putida GR12-2 *J. Bacteriol.* **186** 5661–71
[15] Robinson C H 2001 Cold adaptation in Arctic and Antarctic fungi *New Phytologist* **151** 341–53
[16] Huang T, Nicodemus J, Zarka D G, Thomashow M F, Wisniewski M and Duman J G 2002 Expression of an insect (Dendroides canadensis) antifreeze protein in Arabidopsis thaliana results in a decrease in plant freezing temperature *Plant Mol. Biol.* **50** 333–44
[17] Hew C, Poon R, Xiong F, Gauthier S, Shears M, King M, Davies P and Fletcher G 1999 Liver-specific and seasonal expression of transgenic Atlantic salmon harboring the winter flounder antifreeze protein gene *Transgenic Res.* **8** 405–14
[18] Griffith M and Ewart K V 1995 Antifreeze proteins and their potential use in frozen foods *Biotechnol. Adv.* **13** 375–402
[19] Breton G, Danyluk J, Ouellet F and Sarhan F 2000 Biotechnological applications of plant freezing associated proteins *Biotechnol. Annu. Rev.* **6** 59–101
[20] Rubinsky B, Arav A and Devries A L 1992 The cryoprotective effect of antifreeze glycopeptides from Antarctic fishes *Cryobiology* **29** 69–79
[21] Li B and Sun D W 2002 Novel methods for rapid freezing and thawing of foods—a review *J. Food Eng.* **54** 175–82
[22] Raymond J A and DeVries A L 1977 Adsorption inhibition as a mechanism of freezing resistance in polar fishes *Proc. Natl Acad. Sci. USA* **74** 2589–93
[23] Knight C A 2000 Structural biology. Adding to the antifreeze agenda *Nature* **406** 249–51
[24] Sander L M and Tkachenko A V 2004 Kinetic pinning and biological antifreezes *Phys. Rev. Lett.* **93** 128102
[25] Knight C A, Devries A L and Oolman L D 1984 Fish antifreeze protein and the freezing and recrystallization of ice *Nature* **308** 295–6
[26] Pertaya N, Marshall C B, DiPrinzio C L, Wilen L, Thomson E, Wettlaufer J S, Davies P L and Braslavsky I 2007 Fluorescence microscopy evidence for quasi-permanent attachment of antifreeze proteins to ice surfaces *Biophys. J.* **92** 3663–74

[27] Graether S P, Kuiper M J, Gagne S M, Walker V K, Jia Z, Sykes B D and Davies P L 2000 Beta-helix structure and ice-binding properties of a hyperactive antifreeze protein from an insect *Nature* **406** 325–8
[28] Marshall C B, Daley M E, Sykes B D and Davies P L 2004 Enhancing the activity of a beta-helical antifreeze protein by the engineered addition of coils *Biochemistry* **43** 11637–46
[29] Marshall C B, Chakrabartty A and Davies P L 2005 Hyperactive antifreeze protein from winter flounder is a very long rod-like dimer of alpha-helices *J. Biol. Chem.* **280** 17920–9
[30] Gauthier S Y, Marshall C B, Fletcher G L and Davies P L 2005 Hyperactive antifreeze protein in flounder species: the sole freeze protectant in American plaice *FEBS J.* **272** 4439–49
[31] Scotter A J, Marshall C B, Graham L A, Gilbert J A, Garnham C P and Davies P L 2006 The basis for hyperactivity of antifreeze proteins *Cryobiology* **53** 229–39
[32] Pertaya N, Marshall C B, Celik Y, Davies P L and Braslavsky I 2007 Direct visualization of spruce budworm antifreeze protein bound to an ice crystal: basal plane binding confers hyperactivity, in preparation
[33] Schewe P F, Stein B P and Schwarzchild B 2007 Physics updates: hyperactive antifreeze proteins *Phys. Today* **60** 23–4
[34] Bar M, Pertaya N, Celik Y, Choi Y E, Davies P L, Fass D and Braslavsky I 2007 Growth habits of ice under the influence of Tenebrio molitor ice binding protein, in preparation
[35] Maruyama M 2005 Roughening transition of prism faces of ice crystals grown from melt under pressure *J. Cryst. Growth* **275** 598–605
[36] Chakrabartty A and Hew C L 1991 The effect of enhanced alpha-helicity on the activity of a winter flounder antifreeze polypeptide *Eur. J. Biochem.* **202** 1057–63
[37] Leinala E K, Davies P L, Doucet D, Tyshenko M G, Walker V K and Jia Z 2002 A beta-helical antifreeze protein isoform with increased activity. Structural and functional insights *J. Biol. Chem.* **277** 33349–52
[38] Kuiper M J, Lankin C, Gauthier S Y, Walker V K and Davies P L 2003 Purification of antifreeze proteins by adsorption to ice *Biochem. Biophys. Res. Commun.* **300** 645–8
[39] Carmi Y, Polturak E and Lipson S G 1989 Roughening transition in dilute He-3–He-4 mixture crystals *Phys. Rev. Lett.* **62** 1364–7
[40] Avron J E, Balfour L S, Kuper C G, Landau J, Lipson S G and Schulman L S 1980 Roughening transition in the He-4 solid–superfluid interface *Phys. Rev. Lett.* **45** 814–7
[41] Balibar S, Alles H and Parshin A Y 2005 The surface of helium crystals *Rev. Mod. Phys.* **77** 317–70
[42] Wettlaufer J S 2001 Dynamics of ice surfaces *Interface Sci.* **9** 117–29
[43] Raymond J A, Wilson P and DeVries A L 1989 Inhibition of growth of nonbasal planes in ice by fish antifreezes *Proc. Natl Acad. Sci. USA* **86** 881–5
[44] Graham L A, Liou Y C, Walker V K and Davies P L 1997 Hyperactive antifreeze protein from beetles *Nature* **388** 727–8
[45] Strom C S, Liu X Y and Jia Z C 2005 Why does insect antifreeze protein from Tenebrio molitor produce pyramidal ice crystallites? *Biophys. J.* **89** 2618–27
[46] Wathen B, Kuiper M, Walker V and Jia Z 2003 A new model for simulating 3d crystal growth and its application to the study of antifreeze proteins *J. Am. Chem. Soc.* **125** 729–37